


Antiferromagnetism-Induced Spin Splitting in Systems Described by Magnetic Layer Groups

Sergei A. Egorov,* Daniel B. Litvin, and Robert A. Evarestov*

 Cite This: *J. Phys. Chem. C* 2021, 125, 16147–16154

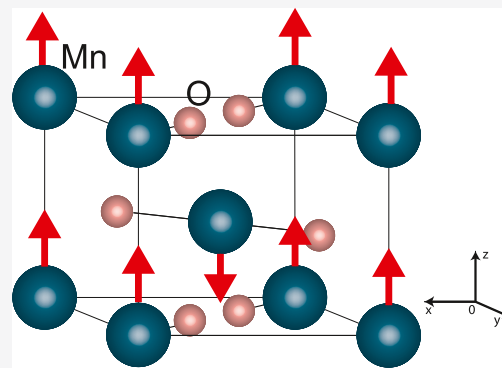
 Read Online

ACCESS |

 Metrics & More

 Article Recommendations

ABSTRACT: In this paper, we report the classification of all the 528 magnetic layer groups into seven spin splitting prototypes, in analogy to the similar classification previously reported for the 1651 magnetic space groups [Yuan et al., *Phys. Rev. Mat.* 2021, 5, 014409]. According to this classification, induced (Pekar–Rashba) spin splitting is possible in the antiferromagnetic monolayers described by magnetic layer groups of type I (no anti-unitary operations) and III, both in the presence and in the absence of the space inversion operation. As one specific application, we have studied theoretically the (110) monolayer of antiferromagnetic (AFM) MnO_2 . Our density functional theory calculations for this structure predicted colossal (on the order of 1 eV) spin splitting in the entire Brillouin zone, similar to the case of the (110) monolayer of AFM MnF_2 which was studied by us earlier. This splitting is much larger compared to the corresponding values for the bulk AFM1 structure of $\beta\text{-MnO}_2$, which was rationalized by noting that the (110) monolayer is described by the type I magnetic layer group that does not contain anti-unitary symmetry operations, and therefore, spin splitting is not suppressed anywhere in the entire Brillouin zone, including high-symmetry points and lines.



1. INTRODUCTION

The ability to create and control the spin polarization of electrons in solids constitutes one of the central goals of the rapidly developing field of spintronics.^{1–3} The use of antiferromagnets (AFMs) represents a promising direction for achieving this goal due to the absence of stray fields in the AFM compounds.^{4–7} The main mechanism for achieving the required spin splitting (SS) is the spin–orbit coupling (SOC), whose strength in crystals is quantified via wavevector-dependent band SS.^{4–7}

In a recent ground-breaking theoretical study,⁴ the joint effect of two SOC mechanisms, electric^{8,9} and magnetic,¹⁰ has been considered in the analysis of SS in the AFM phase of the bulk MnF_2 . The major difference between the two SOC mechanisms can be briefly summarized as follows: the electric (Rashba–Dresselhaus)^{8,9} mechanism of SOC couples Pauli spin matrices to the electron momentum $\hbar\mathbf{k}$, while the magnetic (Pekar–Rashba)¹⁰ mechanism couples Pauli spin matrices to the electron coordinate \mathbf{r} . The central finding of the study⁴ was the giant magnetically induced SS (on the order of several hundreds of meV) found for the bulk AFM phase of MnF_2 .

The important finding of ref 4, which has very significant implications for the field of AFM spintronics, has been subsequently generalized in ref 11 by performing a detailed group-theoretical-based symmetry analysis of the AFM-induced SS. To this end, all the 1651 magnetic space groups

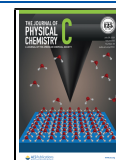
(MSGs)¹² have been divided into seven SS prototypes, from SST-1 to SST-7.¹¹ In this process, it was determined that 422 MSGs could support the magnetically induced SS.¹¹

While the important work of refs 4 and 11 has focused on bulk AFM compounds (both in the presence and in the absence of the electric Rashba–Dresselhaus SOC), it is also of great interest to study SS in *monolayer structures*, which are of major importance for a variety of scientific and technological applications, such as photocatalysis,^{13–15} the injection of spin-polarized electrons across interfaces,¹⁶ and spintronic devices.¹⁷ Along these lines, in our recent study¹⁸ we have reported on the colossal SS (on the order of several electronvolts, i.e., an order of magnitude larger compared to the giant SS reported in refs 4 and 11) that was discovered in the (110) collinear AFM monolayer of MnF_2 ; the latter effect was observed in the absence of the electric Rashba–Dresselhaus SOC and was due to the magnetic Pekar–Rashba SOC. Furthermore, in the bulk structure of AFM MnF_2 , the vanishing of SS is imposed by strict symmetry requirements at

Received: March 24, 2021

Revised: July 5, 2021

Published: July 16, 2021



certain high-symmetry points and lines of the bulk crystal 3D Brillouin zone, such as Γ , M , X , Z , and A points, and Γ – X line. The vanishing of the SS for the aforementioned high-symmetry points and lines likely results in the suppression of its magnitude in the neighboring parts of the bulk crystal 3D Brillouin zone, where it is allowed by symmetry. By contrast, the (110) collinear AFM monolayer of MnF_2 is described by a Fedorov-type magnetic layer group,¹² which does not contain any anti-unitary operations.¹⁸ As a result, the Pekar–Rashba¹⁰ AFM-induced SS does not become suppressed anywhere in the 2D Brillouin zone of the monolayer and exceeds by at least an order of magnitude the SS observed in the bulk structure of AFM MnF_2 .

The robustness of the above finding of ref 18 has been confirmed by density functional theory (DFT) calculations of the wavevector-dependent band SS for the (110) AFM monolayer of MnF_2 using two different functionals: M06¹⁹ and B1WC²⁰ were used in our calculations. The former functional¹⁹ belongs to the family of hybrid meta exchange–correlation functionals which can be used for description of both covalent and noncovalent bonds. The latter functional²⁰ was successfully used²¹ to calculate the magnetic effects on the infrared phonon spectra of MnF_2 . In all the calculations, the full geometry optimization was made, and the magnitude of SS was found to be very similar in both sets of calculations.¹⁸

Given the large magnitude of SS found for the (110) collinear AFM monolayer of MnF_2 , it would be of importance to generalize the results of ref 18 by formulating the group-theoretical symmetry-based conditions for the observation of magnetically induced SS in the AFM monolayer structures. To this end, following the procedure developed in ref 11 for the 1651 MSGs, one would need to divide all the 528 magnetic layer groups²² into SS prototypes, with the primary goal of determining which of these groups could support the magnetically induced SS. This is the central purpose of the present work. Such an opportunity exists because any magnetic layer group is a subgroup of a MSG.²³

The remainder of the paper is organized as follows. In Section 2, we formulate the seven SS prototypes for the monolayers and indicate which of these prototypes could support magnetically induced SS. In Section 3, we classify all the 528 magnetic layer groups²² into seven SS prototypes defined in Section 2. In Section 4, we provide DFT calculation results and group-theoretical analysis of magnetically induced Pekar–Rashba SS in the bulk structure of MnO_2 . In Section 5, we present DFT calculation results and group-theoretical analysis of magnetically induced Pekar–Rashba SS in the (110) monolayer of MnO_2 . In Section 6, we conclude.

2. AFM-INDUCED SPIN SPLITTING: SYMMETRY CONDITIONS

The 1651 MSGs were employed in previous theoretical work on SS in bulk AFMs^{4–7,11} and can be classified into four types:¹² 230 MSGs of type I (Fedorov-type groups), which contain unitary symmetry operations *only*, 230 MSGs of type II (gray groups describing nonmagnetic compounds), where for each unitary symmetry operation R , there is a corresponding anti-unitary symmetry operation θR (θ being the anti-unitary time-reversal operation), 517 MSGs of type III, and 674 MSGs of type IV (both in type III and in type IV MSG groups, the unitary part is the invariant subgroup of MSG of index 2, containing half of its spatial symmetry operations keeping the crystalline atomic structure invariant). The key difference

between MSGs of type III and IV is that the former do not contain anti-unitary symmetry operation θT (T being a translation), while the latter do contain θT symmetry operations.¹² The MSGs of type II can only correspond to nonmagnetic compounds, while AFM compounds can be described by MSGs of type I, III, or IV, depending on whether the anti-unitary symmetry operations are completely absent (type I), are present but do not contain operations θT (type III), or are present and do contain operations θT (type IV).^{11,12} In ref 11, the 1651 MSGs were further classified by identifying seven SS prototypes (SSTs), including four AFM prototypes, one ferromagnetic (FM) prototype, and two nonmagnetic (NM) prototypes.¹¹

Similar to MSGs, 528 magnetic layer groups (MLGs) can be classified into the same four types:²² 80 MLGs of type I (colorless Fedorov-type groups), which contain unitary symmetry operations *only*, 80 MLGs of type II (gray groups describing nonmagnetic compounds), where for each unitary symmetry operation R , there is a corresponding anti-unitary symmetry operation θR , 246 MLGs of type III, and 122 MLGs of type IV (in both type III and type IV MLG groups, the unitary part is the invariant subgroup of MLG of index 2, containing half of its spatial symmetry operations keeping the crystalline atomic structure invariant). The key difference between MLGs of type III and IV is that in the former case, the monolayer has a two-periodic (2D) Bravais lattice with the magnetic 2D unit cell being equivalent to the crystallographic 2D unit cell, while in the latter case, the monolayer has a 2D Bravais lattice with the magnetic 2D unit cell being the supercell of the crystallographic 2D unit cell.²² Following the general approach outlined in ref 11 for classifying 1651 MSGs into seven SSTs, in the present work, we have developed a similar classification of 528 MLGs into seven SSTs with the goal of analyzing SS in monolayer systems. Here, we give a list of these seven SSTs with a brief description of each prototype, while in Section 3, we provide Table 1 where all the 528 MLGs²² are classified according to the seven SSTs listed below.

SST-1 corresponds to AFM compounds that are described by magnetic layer groups of type III, that is, their magnetic 2D primitive unit cell is equivalent to the nonmagnetic 2D primitive unit cell. The criterion for the SST-1 prototype is the presence of the inversion operation combined with time-reversal ($\bar{1}'$) in the magnetic layer group, which precludes both electrically (Rashba–Dresselhaus) and magnetically (Pekar–Rashba) induced SS.

SST-2 corresponds to AFM compounds that are described by magnetic layer groups of type IV, that is, their magnetic primitive unit cell is a supercell of the nonmagnetic primitive unit cell. The criterion for the SST-2 prototype is the presence of the inversion operation $\bar{1}$ in the magnetic layer group, which precludes both electrically (Rashba–Dresselhaus) and magnetically (Pekar–Rashba) induced SS.

SST-3 corresponds to AFM compounds that are described by magnetic layer groups of type IV that do not contain the operation $\bar{1}$. In these compounds, only electrically induced (Rashba–Dresselhaus) SS is possible and is proportional to the strength of the SOC.

SST-4A corresponds to AFM compounds that are described by magnetic layer groups of either type I or type III that contain the inversion operation $\bar{1}$ but not the space inversion operation combined with time-reversal ($\bar{1}'$). In these compounds, magnetically induced Pekar–Rashba SS is

Table 1

type	MLG
SST-1, MLG type III, contains \bar{I}'	2.3, 6-7.3-4, 14.3-4, 15.3, 15.5, 16.3, 16.5, 17.3, 17.5, 18.3, 18.5, 37.3, 37.6-7, 38.3, 38.7-9, 39.3, 39.6-7, 40.3, 40.7-9, 41.3, 41.7-9, 42.3, 42.7-9, 43.3, 43.7-9, 44.3, 44.6-7, 45.3, 45.7-9, 46.3, 46.6-7, 47.3, 47.6-7, 48.3, 48.6-7, 51-52.3-4, 61.3, 61.5-7, 62.3, 62.5-7, 63.3, 63.5-7, 64.3, 64.5-7, 66.3, 71.3, 71.5, 72.3, 72.5, 75.3, 75.5, 80.3, 80.5, 80.8-9
SST-2, MLG type IV, contains \bar{I}	2.4, 6.6-7, 7.6, 14.6-10, 15-16.6-7, 18.6-9, 37.8-13, 38.10-13, 40-41.10-13, 47.8-13, 48.8-11, 51.6-7, 61.10-13
SST-3, MLG type IV, does not contain \bar{I}	1.3, 3.4, 4.4-5, 5.4, 8.4-7, 9.4, 10.4-5, 11.4-7, 12.4, 13.4-5, 19.5-7, 20.6-7, 22-23.5-7, 24.6-7, 26.5-7, 27.6-13, 28-30.6-7, 31.6-9, 35-36.6-9, 49-50.4, 53.6-7, 55.6-7, 57.6-7, 59.6-7
SST-4A and SST-5, MLG type I, contain \bar{I} , does not contain \bar{I}'	2.1, 6.1, 7.1, 14-18.1, 37-48.1, 51-52.1, 61-64.1, 66.1, 71-72.1, 75.1, 80.1
SST-4A and SST-5, MLG type III, contain \bar{I} , does not contain \bar{I}'	6-7.5, 14.5, 15-18.4, 37.4-5, 38.4-6, 39.4-5, 40-43.4-6, 44.4-5, 45.4-6, 46-48.4-5, 51-52.5, 61.4, 61.8-9, 62.4, 62.8-9, 63.4, 63.8-9, 64.4, 64.8-9, 71-72.4, 75.4, 80.4, 80.6-7
SST-4B and SST-5, MLG type I, does not contain \bar{I} or \bar{I}'	1.1, 3-5.1, 8-13.1, 19-36.1, 49-50.1, 53-60.1, 65.1, 67-70.1, 73-74.1, 76-79.1
SST-4B and SST-5, MLG type III, does not contain \bar{I} or \bar{I}'	3-5.3, 8-13.3, 19.3-4, 20.3-5, 21-23.3-4, 24.3-5, 25-26.3-4, 27-36.3-5, 49-50.3, 53-60.3-5, 67-70.3, 73-74.3, 76-79.3-5
SST-6, MLG type II, contains \bar{I}	2.2, 6-7.2, 14-18.2, 37-48.2, 51-52.2, 61-64.2, 66.2, 71-72.2, 75.2, 80.2
SST-7, MLG type II, does not contain \bar{I}	1.2, 3-5.2, 8-13.2, 19-36.2, 49-50.2, 53-60.2, 65.2, 67-70.2, 73-74.2, 76-79.2

possible both in the absence and in the presence of the electrically induced (Rashba–Dresselhaus) SOC.

SST-4B corresponds to AFM compounds that are described by magnetic layer groups of either type I or type III that contain neither the inversion operation nor \bar{I} the inversion operation combined with time reversal (\bar{I}'). In these compounds, magnetically induced Pekar–Rashba SS is possible both in the absence and in the presence of the electrically induced (Rashba–Dresselhaus) SOC.

SST-5 corresponds to FM compounds that are described by magnetic layer groups of either type I or type III that do not contain the inversion operation combined with time-reversal (\bar{I}'). Magnetically induced SS is possible in these compounds, both in the presence and in the absence of the inversion operation \bar{I} .

SST-6 corresponds to NM compounds that are described by magnetic layer groups of type II that contain the inversion operation \bar{I} . No SS is possible in these compounds.

SST-7 corresponds to NM compounds that are described by magnetic layer groups of type II that do not contain the inversion operation \bar{I} . Only electrically induced Rashba–Dresselhaus SS is possible in these compounds.

Given that the main focus of the present work is on the magnetically induced (Pekar–Rashba) SS in the AFM monolayers, we will be primarily concerned with SST-4A and SST-4B prototypes, that is, magnetic layer groups of either type I or type III, which either contain (SST-4A) or do not contain (SST-4B) the inversion operation.

3. CLASSIFICATION OF MAGNETIC LAYER GROUPS

In this section, we provide in Table 1 the classification of the 528 magnetic layer groups according to the spin-splitting prototypes SST-1 to SST-7 listed in Section 2. The magnetic layer groups are listed according to the first two numerals of their serial number in the survey of magnetic layer group types given in the book Magnetic Group Tables.²² For reasons of compactness, consecutive sequences of groups are abbreviated, for example, the symbol 38.7–9 denotes the groups 38.7, 38.8, and 38.9; 51–52.3–4 denotes the groups 51.3, 52.3, 51.4, and 52.4. The Opechowski–Guccione (OG) style notation of these magnetic layer groups is given in the same survey of magnetic layer group types.²² The Belov–Nerenova–Smirnova (BNS) style notation of these magnetic layer groups is identical for type I, II, and III magnetic groups. The symbols for type IV magnetic layer groups in BNS notation can be found in the comparison of OG and BNS magnetic group-type symbols in the Magnetic Group Tables book,²² for example, the magnetic layer group 48.10 is $c_pmm'e'$ in OG notation and p_maa in BNS notation.

4. β -MNO₂ BULK STRUCTURE: DFT CALCULATIONS AND SPIN SPLITTING ANALYSIS

4.1. DFT Calculations. Manganese dioxide MnO₂ is a very promising electrode material due to its low cost, low toxicity, and easy preparation.²⁴ As such, this material has been extensively studied theoretically.^{25–28} In the present work, we have performed the first-principle linear combination of atomic orbital calculations of MnO₂ using the CRYSTAL17 code in the periodic model.²⁹ The all-electron basis sets for Mn and O atoms have been chosen³⁰ from the site <https://www.crystal.unito.it/basis-sets.php> in the form of all-electron triple-zeta valence basis sets augmented by one set of polarization

functions. The hybrid DFT functional M06¹⁹ was used in our calculations. This functional¹⁹ belongs to the family of hybrid meta exchange–correlation functionals which can be used for description of both covalent and noncovalent bonds. In all the calculations, the full geometry optimization was made.

The evaluation of the Coulomb series and the exchange series has been done with the accuracy controlled by a set of tolerances, which were taken to be (10^{-7} , 10^{-7} , 10^{-7} , 10^{-7} , and 10^{-14}). The integration in the Brillouin zone has been performed using the Monkhorst–Pack scheme for an 8 by 8 by 8 k -point mesh.³¹

In order to validate our computational approach, we begin by considering the bulk structure of the β -MnO₂ crystal, where the experimental structural data³² provide useful reference. The results of our first-principles calculations are summarized in Table 2, which gives the structural parameters, Mn atomic

charge, Mn magnetic moment, and relative (to NM state) energies for different magnetic orderings for the bulk β -MnO₂ crystal: NM state, three antiferromagnetic states (AFM1, AFM2, and AFM3 discussed below), and FM state. Experimental structural data are taken from Ref.;³² experimental magnetic moment is taken from Ref 33.

We considered three different AFM magnetic orderings for the bulk β -MnO₂ crystal. In the simplest AFM1 arrangement, the two Mn atoms of the unit cell of the rutile structure are aligned anti-parallel, that is, α and β Mn atom spin projections are collinear (see Figure 1). It means that the superexchange interaction exists between the neighboring corner cation and body center cation. AFM1 arrangement is experimentally found and theoretically confirmed for the rutile structure of bulk MnF₂.¹⁸ AFM2 arrangement corresponds to the superexchange interaction between two Mn atoms neighboring along the c -axis. In ref 38, a third type of spin arrangement was proposed for bulk β -MnO₂—a screw-type magnetic structure with helically ordered magnetic moments. In this case, the magnetic unit cell is seven times larger along the c -axis than the chemical unit cell and all the spins are aligned parallel in the c -plane and screw with pitch $7/2c$. We denote this structure AFM3. The AFM3 structure is not yet fully understood,²⁶ and therefore, the previously published β -MnO₂ calculations were performed only for the AFM1 structure.^{25–28} MSGs of AFM1 and AFM2 arrangements belong to types III and IV, respectively. The NM phase and FM ordering is considered only for the rutile structure with two Mn atoms in the unit cell. From Table 2, it is seen that the AFM1 structure is the most stable one (ΔE is the energy difference per formula unit taken by zero for NM magnetic ordering). The calculated structural parameters for the AFM1 arrangement are the closest to the experimental ones, but do not differ strongly for all three AFM

Table 2. Lattice Constants a and c (Measured in Å), Positional Parameter u for O Anions, Charge q on the Mn Cation, Magnetic Moment on the Mn Cation (Measured in μ_B , Aligned along the Tetragonal [001] Axis), and Energies ΔE (in eV) per Formula Unit Relative to the NM State^a

magnetic state	a , Å	c , Å	u	q (Mn)	magn. mom., μ_B	ΔE (eV)
NM	4.456	2.647	0.2906	1.28		0
AFM1	4.394	2.881	0.3056	1.56	3.07	−3.05
AFM2	4.337	2.910	0.3071	1.53	3.21	−1.64
AFM3	4.397	2.880	0.3060	1.56	3.05–3.10	−3.00
FM	4.358	2.842	0.2963	1.40	1.0	−0.79
Expt.	4.398	2.873			2.40	

^aThe DFT results are given for the functional M06;¹⁹ experimental data in the last row are taken from refs 32 and 33.

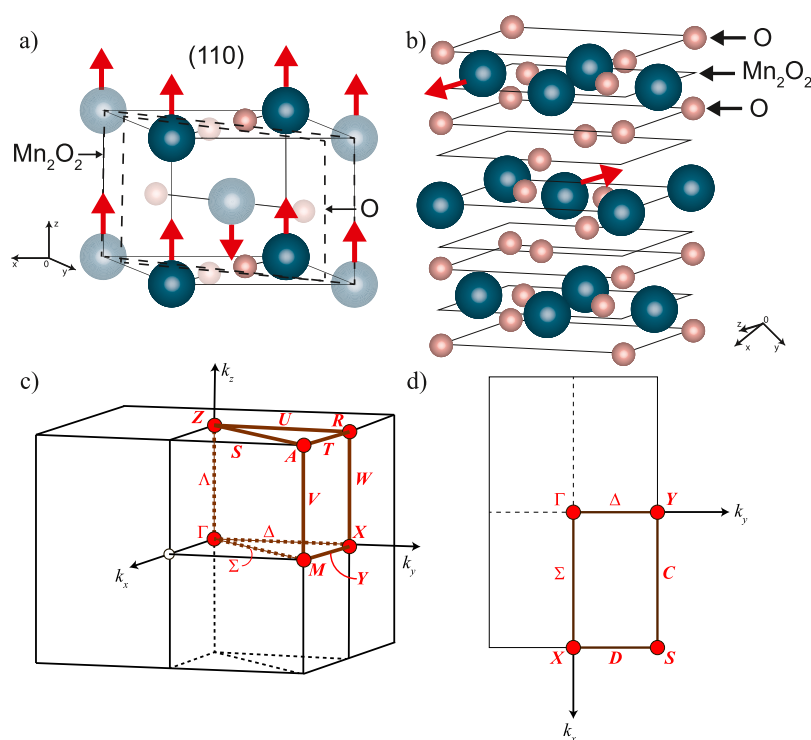


Figure 1. (a) AFM1 bulk MnO₂; (b) (110) AFM monolayer MnO₂; (c) Brillouin zone with high-symmetry points for the space group no 136 $P4_2/mnm$; (d) Brillouin zone with high-symmetry points for the layer group no 37 $pmmn$. Brillouin zone pictures are taken from the Bilbao Crystallographic Server site.^{34–37}

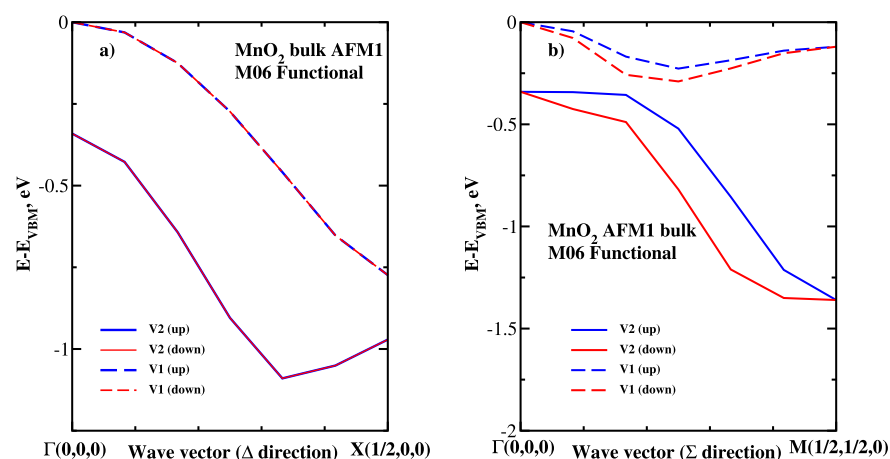


Figure 2. (a) DFT band structure of AFM1 bulk MnO_2 without SOC along the wave-vector Δ -direction Γ – X ; (b) DFT band structure of AFM1 bulk MnO_2 without SOC along the wave-vector Σ -direction Γ – M .

Table 3. Lattice Constants a and b (Measured in Å), Positional Parameter u , Charge q on the Mn Cation, Magnetic Moment on the Mn Cation for Free-Standing Monolayers (hkl), the Energy Difference ΔE between AFM and NM Orderings, and the Energy Difference ΔE_1 between AFM Layer Energies [the Highest Energy is for the Layer (001) and It is Set Equal to 0]

layer (hkl)	a , Å	b , Å	u	q (Mn)	magn. mom., μ_B	ΔE , eV	ΔE_1 , eV
(110)	2.857	6.207	0.3055	1.56	3.42	−0.06	−0.54
(100)	2.809	4.271	0.2743	1.63	3.80	−2.22	−0.49
(101)	3.543	4.676	0.3494	1.58	3.89	−3.20	−0.18
(001)	4.332	4.332	0.2766	1.66	2.76	−1.81	0.0

arrangements considered here. The Mn atomic charges are also close for AFM1–AFM3 orderings and demonstrate essentially covalent Mn–O interaction. The magnetic moments for AFM configurations are close to $3 \mu_B$ and agree with those found in other AFM1 calculations reported in the literature ($2.89 \mu_B$ from PBE0 calculations²⁶ and $2.96 \mu_B$ from GGA + U + J calculations²⁷) and are close to an experimental value of $2.40 \mu_B$.³³

According to ref 4, SS is absent in the calculations without electrically induced SOC for MSG of type IV, that is, AFM2 magnetic ordering. According to our DFT calculations (not shown), in the screw-type AFM3 arrangement, SS is close to that found for AFM1 orderings; the corresponding values of ΔE are also close; see Table 2.

4.2. SS Analysis. The conclusions of Section 4.1 are confirmed in our SS calculations. Specifically, Figure 2 shows our DFT results for the two upper valence bands V1 and V2 (both for spin-up and spin-down electrons) obtained for the bulk AFM1 MnO_2 without electrically induced SOC. The results are shown for two wave-vector paths in the 3D Brillouin zone (see Figure 1c): Δ -direction Γ – X (panel a) and Σ -direction Γ – M (panel b). Similar to the bulk AFM structure of MnF_2 analyzed in our previous work,¹⁸ the AFM1 bulk structure of MnO_2 is described by MSG no 498, which belongs to type III. Thus, the group theoretical analysis of SS reported earlier^{4,18} for MnF_2 can be applied directly to the AFM1 bulk structure of MnO_2 . In particular, SS is strictly forbidden by symmetry along the path Γ – X ,^{4,18} and indeed, one sees that spin-up and spin-down bands coincide in Figure 2a for all the wave vectors. On the other hand, along the path Γ – M (Figure 2b), there is significant k -dependent SS present—approximately 20 meV (at the largest) between V1 up and down bands and approximately 250 meV (at the largest) between V2 up and down bands. These numbers are somewhat different

from the corresponding numbers reported¹⁸ for MnF_2 , which is due to the chemical composition difference between the two compounds.

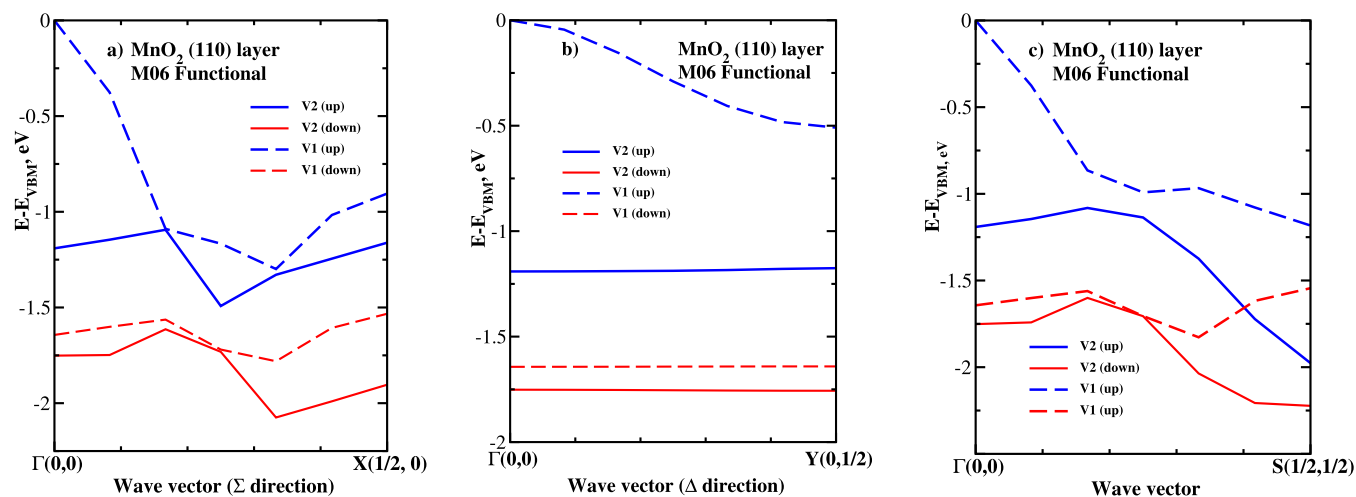
Given that the AFM2 bulk structure is described by MSG of type IV, magnetically induced Pekar–Rashba SS is prohibited by symmetry here, and indeed, our DFT calculations have shown that spin-up and spin-down bands coincide in for all the wave vectors considered (plot not shown here). Finally, the magnitude of SS for the AFM3 bulk structure obtained from our DFT calculations is similar to the values observed in Figure 2 and is not shown here.

5. MnO_2 MONOLAYERS: DFT CALCULATIONS AND GROUP-THEORETICAL ANALYSIS OF SPIN-SPLITTING

5.1. DFT Calculations. The surfaces of β - MnO_2 hold great potential for high electrochemical and catalytic performance³⁹ and have received significant theoretical attention.⁴⁰ An extensive DFT-based study of several atomically thin AFM monolayers has been recently reported,⁴¹ although no group-theoretical analysis of their magnetic structure has been carried out. By contrast, in our calculational approach, the monolayers are not atomically thin, but rather consist of two nearest atomically thin planes and contain two formula units. The results of our DFT calculations for MnO_2 monolayers are given in Table 3. From the last column of Table 3, one sees that in our M06 calculations, the (110) layer is the most favorable energetically. Atomic charges (ranging from 1.56 to 1.66) demonstrate covalent nature of Mn–O interactions, as was already found for the bulk β - MnO_2 (see Table 2). The magnetic moments on Mn atoms are similar for all the layers considered. As the results of our bulk calculations indicate that the SS splitting in bulk β - MnO_2 is defined by AFM1 spin arrangement, we consider SS for the MnO_2 -based monolayers

Table 4. International Symbols and the Numbers of NMLGs (from the Bilbao Crystallographic Server)⁴⁵ and AFMLGs²² as Discussed in the Text

layer (<i>hkl</i>)	location	NMLG symbol	NMLG number	AFMLG number	AFMLG symbol	unitary subgroup symbol	SST (type)
(110)	[0d, 1/2d], d = a + b	<i>pmmm</i>	37	37.1.230	<i>pmmm</i>	<i>pmmm</i>	4A (I)
(100)	[1/4d, 3/4d], d = a	<i>pm2₁n</i>	32	32.5.201	<i>pm2₁'n'</i>	<i>pm</i>	4B (III)
(101)	[0d, 1/2d], d = a	<i>p2₁/b</i>	17	17.4.93	<keep-together> <i>p2₁'/b'</i> </keep-together>	<i>p1</i>	4A (III)
(001)	[1/4d, 3/4d], d = c	<i>p4₂m</i>	58	58.3.407	<i>p4₂'m'</i>	<i>p4</i>	4B (III)

**Figure 3.** (a) DFT (functional M06) band structure of AFM (110) monolayer MnO₂ without SOC along the wave-vector direction Γ -X; (b) DFT (functional M06) band structure of AFM (110) monolayer MnO₂ without SOC along the wave-vector direction Γ -Y; (c) DFT (functional M06) band structure of AFM (110) monolayer MnO₂ without SOC along the wave-vector direction Γ -S.

by the same way as it was done for bulk MnF₂-based monolayers in ref 18. The use of CRYSTAL17 code allowed us to determine space and layer groups (both magnetic and NM) for the bulk crystal and four slabs, containing two formula units in 3D and 2D unit cells, respectively.

5.2. MLG Determination. In the present paper, we use a two-step procedure for the search of MLGs for the calculations without electrically induced SOC. This procedure was proposed by us earlier and applied to study MnF₂-based monolayers.¹⁸ It can be applied for calculations with any periodic code giving in the output file the symmetry information. For convenience, we briefly summarize the two steps of this procedure below.

As the **first step**, one finds NM layer groups based on the NM bulk MnO₂ crystal (scanned space group no 136 *P4₂/mnm*). For this, we used the program SECTIONS from Bilbao Crystallographic Server (BCS).^{34–36,42} This program identifies, for a given nonmagnetic space group, the full set of possible NM layer symmetries of periodic sections defined by their common normal vector and located within the unit cell. The program accepts as input a scanned space group given in any arbitrary setting. The results are expressed in both the given basis of the input space group and the standard setting of the corresponding layer groups.

The first column of Table 4 gives (*h,k,l*) for four layers which are cut from the β -MnO₂ bulk structure. Each specific layer is defined by Miller indexes (*h,k,l*), as given in the first column of Table 4. The second column of Table 4 gives the location of the periodic section within the unit cell;²³ **d** is the vector normal to the layer, while **a**, **b**, and **c** are the translation vectors of the scanning group.²³ The output file of the layer structure optimization (performed in the absence of the

electric Rashba–Dresselhaus SOC), given by CRYSTAL17 code, contains the unitary layer group symmetry operations and allows one to choose the appropriate NMLG from those given on the BCS site.^{34–36,42} The third and fourth columns of Table 4 give international symbols and numbers, respectively, of those NMLGs which correspond to the four-layer structures chosen for the MnO₂ NM rutile structure with scanning space group no 136 *P4₂/mnm*.

As the **second step**, we find the antiferromagnetic layer groups (AFMLG) for the chosen monolayers. The CRYSTAL17 code was now used for the structure optimization of magnetic AFM MnO₂ layers. The corresponding CRYSTAL17 output file gives the symmetry operations for the unitary subgroup of the corresponding magnetic layer group. This information was used to find for any layer the corresponding AFMLG from 528 magnetic layer groups given in Magnetic Group Tables.^{22,43,44} The corresponding results are given in the columns 5–7 of Table 4. As discussed earlier, the AFM monolayer compounds can only be described by MLGs of type I, III, and IV. In column 5 of Table 4, we give both the number of the AFMLG according to the Magnetic Group Tables.²² We point out that according to the classification scheme adopted in the Magnetic Group Tables,²² the numbers of the type XX.1.XX always correspond to type I MLGs, while the numbers of the type XX.2.XX always correspond to type II MLGs. In order to distinguish between types III and IV MLGs, one needs to look at the symmetry operations listed in the Magnetic Group Tables²² and check whether symmetry operations of type θT are present (type IV) or not (type III).

Following this procedure, one finds that monolayers (100), (101), and (001) are characterized by MLGs of type III, while the monolayer (110) is characterized by MLG of type I, that is,

all-unitary Fedorov-type group 37.1.230. As discussed above, the fundamental difference between MLGs of type I and III is the complete absence of antiunitary symmetry operations in the former groups, while in the latter groups, such operations are present and are likely to impose the strict symmetry requirement of vanishing SS for certain high-symmetry points and lines of the Brillouin zone. As a result, the magnitude of SS becomes suppressed over the entire Brillouin zone for the monolayers described by MLGs of type III. By contrast, in the monolayer (110) characterized by MLG of type I, the vanishing of SS is not required by symmetry *anywhere* in the Brillouin zone. As a result, the Pekar–Rashba¹⁰ AFM-induced SS does not become suppressed and exceeds by at least an order of magnitude both the SS observed in the bulk structure of AFM MnO₂ (described by MSG of type III), as well as SS observed for other monolayers considered here, which are described by MLGs of type III (in the areas of the 2D Brillouin zone where it is not prohibited by symmetry requirements). Both SST (according to Table 1) and the MLG type are given in the last column of Table 4.

5.3. AFM Spin Splitting in MnO₂ Monolayers. Figure 3 shows our DFT results for the top two valence bands V1 and V2 (both for spin-up and spin-down electrons) obtained for the AFM (110) monolayer MnO₂ without SOC (with functional M06). The results are shown for three wave-vector paths in the Brillouin zone (see Figure 1d): Σ direction Γ – X (panel a), Δ direction Γ – Y (panel b), and direction Γ – S (panel c). One observes SS for *all* wave vectors, including high-symmetry points Γ , X , and M , which is in stark contrast to the bulk case, where SS is typically not present at high symmetry points (see Figure 2). Furthermore, the magnitude of SS in the monolayer (around 1 eV) is colossal compared to the bulk values (around 200 meV). In our opinion, the physical origin of this dramatic difference between the monolayer and the bulk behavior, as well as the absence of colossal SS for other monolayers considered here (results not shown), can be understood by considering the symmetry constraints on the SS for various monolayers arising from group-theoretical analysis presented above (see discussion of Table 4).

Specifically, one finds that monolayers (100), (101), and (001) are characterized by MLGs of type III, while the monolayer (110) is characterized by MLG of type I, that is, all-unitary Fedorov-type group 37.1.230. As discussed above, the fundamental difference between MLGs of type I and III is the complete absence of antiunitary symmetry operations in the former groups, while in the latter groups, such operations are present and are likely to impose the strict symmetry requirement of vanishing SS for certain high-symmetry points and lines of the Brillouin zone. As a result, the magnitude of SS becomes suppressed over the entire Brillouin zone for the monolayers described by MLGs of type III. By contrast, in the monolayer (110) characterized by MLG of type I, the vanishing of SS is not required by symmetry *anywhere* in the Brillouin zone. As a result, the Pekar–Rashba¹⁰ AFM-induced SS does not become suppressed and exceeds by at least an order of magnitude both the SS observed in the bulk structure of AFM MnO₂ (described by MSG of type III) and SS observed for other monolayers considered here, which are described by MLGs of type III (in the areas of the 2D Brillouin zone where it is not prohibited by symmetry requirements).

6. CONCLUSIONS

The major result of the present study is the classification of all the 528 magnetic layer groups into seven SS prototypes summarized in Table 1. Given that the main focus of the present work is on the magnetically induced (Pekar–Rashba) SS in the AFM monolayers, we were primarily concerned with SST-4A and SST-4B prototypes, that is, magnetic layer groups of either type I or type III, which either contain (SST-4A) or do not contain (SST-4B) the space inversion operation. As one specific application, we have studied theoretically the (110) monolayer of AFM MnO₂. Our DFT calculations for this structure predicted colossal (on the order of 1 eV) SS in the entire BZ, similar to the case of the (110) monolayer of AFM MnF₂ which was studied by us earlier.¹⁸ This splitting is much larger compared to the corresponding values for the bulk AFM1 structure of β -MnO₂, which was rationalized by noting that the (110) monolayer is described by type I MLG that does not contain anti-unitary symmetry operations, and therefore, SS is not suppressed anywhere in BZ, including high-symmetry points and lines.

AUTHOR INFORMATION

Corresponding Authors

Sergei A. Egorov – Department of Chemistry, University of Virginia, Charlottesville, Virginia 22901, United States; Institute of Physics, Johannes Gutenberg University Mainz, 55128 Mainz, Germany; orcid.org/0000-0002-0600-2467; Email: sae6z@virginia.edu

Robert A. Evarestov – Institute of Chemistry, Quantum Chemistry Department, St Petersburg State University, St Petersburg 199034, Russia; Email: r.evarestov@spbu.ru

Author

Daniel B. Litvin – Department of Physics, Eberly College, Penn State University, Reading, Pennsylvania 19610, United States

Complete contact information is available at:

<https://pubs.acs.org/10.1021/acs.jpcc.1c02653>

Notes

The authors declare no competing financial interest.

ACKNOWLEDGMENTS

The authors thank Profs. Alex Zunger and Emmanuel Rashba for numerous helpful discussions. S.A.E. is grateful to the members of the SPICE Spintronics Theory group in JGU-Mainz for many helpful comments. R.A.E. thanks the Computer Center of St. Petersburg University for computer facilities and computational time. There is no funding to declare.

REFERENCES

- (1) Žutić, I.; Fabian, J.; Sarma, S. D. Spintronics: Fundamentals and applications. *Rev. Mod. Phys.* **2004**, *76*, 323–410.
- (2) Jungwirth, T.; Marti, X.; Wadley, P.; Wunderlich, J. Antiferromagnetic spintronics. *Nat. Nanotechnol.* **2016**, *11*, 231–241.
- (3) Baltz, V.; Manchon, A.; Tsoi, M.; Moriyama, T.; Ono, T.; Tserkovnyak, Y. Antiferromagnetic spintronics. *Macromolecules* **2018**, *90*, 015005.
- (4) Yuan, L.-D.; Wang, Z.; Luo, J.-W.; Rashba, E. I.; Zunger, A. Giant momentum-dependent spin splitting in centrosymmetric low- Z antiferromagnets. *Phys. Rev. B* **2020**, *102*, 014422.

- (5) Šmejkal, L.; González-Hernández, R.; Jungwirth, T.; Sinova, J. Crystal time-reversal symmetry breaking and spontaneous Hall effect in collinear antiferromagnets. *Sci. Adv.* **2020**, *6*, No. eaaz8809.
- (6) Hayami, S.; Yanagi, Y.; Kusunose, H. Momentum-Dependent Spin Splitting by Collinear Antiferromagnetic Ordering. *J. Phys. Soc. Jpn.* **2019**, *88*, 123702.
- (7) Hayami, S.; Yanagi, Y.; Kusunose, H. Bottom-up design of spin-split and reshaped electronic band structures in antiferromagnets without spin-orbit coupling: Procedure on the basis of augmented multipoles. *Phys. Rev. B* **2020**, *102*, 144441.
- (8) Rashba, E.; Sheka, V. Symmetry of Energy Bands in Crystals of Wurtzite Type II. Symmetry of Bands with Spin-Orbit Interaction Included. *New J. Phys.* **2015**, *17*, 050202. Originally published in *Fiz. Tverd. Tela: Collected Papers* 2: 62–76, 1959
- (9) Dresselhaus, G. Spin-orbit coupling effects in zinc blende structures. *Phys. Rev.* **1955**, *100*, 580–586.
- (10) Pekar, S. I.; Rashba, E. I. Combined resonance in crystals in inhomogeneous magnetic fields. *J. Exp. Theor. Phys.* **1965**, *20*, 1295–1298.
- (11) Yuan, L.-D.; Wang, Z.; Luo, J.-W.; Zunger, A. Prediction of low- Z collinear and noncollinear antiferromagnetic compounds having momentum-dependent spin splitting even without spin-orbit coupling. *Phys. Rev. Mater.* **2021**, *5*, 014409.
- (12) Bradley, C.; Cracknell, A. *The Mathematical Theory of Symmetry in Solids: Representation Theory for Point Groups and Space Groups*; Oxford University Press: Oxford, 2010.
- (13) Torun, E.; Fang, C. M.; de Wijs, G. A.; de Groot, R. A. Role of Magnetism in Catalysis: RuO₂ (110) Surface. *J. Phys. Chem. C* **2013**, *117*, 6353–6357.
- (14) Noda, Y.; Ohno, K.; Nakamura, S. Momentum-dependent band spin splitting in semiconducting MnO₂: a density functional calculation. *Phys. Chem. Chem. Phys.* **2016**, *18*, 13294–13303.
- (15) Müller, M.; Echenique, P. M.; Sánchez-Portal, D. Key Role of the Surface Band Structure in Spin-Dependent Interfacial Electron Transfer: Ar/Fe(110) and Ar/Co(0001). *J. Phys. Chem. Lett.* **2020**, *11*, 7141–7145.
- (16) Zhang, Y.; Liu, P.; Sun, H.; Zhao, S.; Xu, H.; Liu, Q. Symmetry-Assisted Protection and Compensation of Hidden Spin Polarization in Centrosymmetric Systems. *Chin. Phys. Lett.* **2020**, *37*, 087105.
- (17) Fan, X.; Singh, D. J.; Zheng, W. Valence Band Splitting on Multilayer MoS₂: Mixing of Spin-Orbit Coupling and Interlayer Coupling. *J. Phys. Chem. Lett.* **2016**, *7*, 2175–2181.
- (18) Egorov, S. A.; Evarestov, R. A. Colossal Spin Splitting in the Monolayer of Collinear Antiferromagnet MnF₂. *J. Phys. Chem. Lett.* **2021**, *12*, 2363–2369.
- (19) Zhao, Y.; Truhlar, D. G. The M06 suite of density functionals for main group thermochemistry, thermochemical kinetics, non-covalent interactions, excited states, and transition elements: two new functionals and systematic testing of four M06-class functionals and 12 other functionals. *Theor. Chem. Acc.* **2008**, *120*, 215–241.
- (20) Birc, D. I.; Orlando, R.; Shaltaf, R.; Rignanese, G.-M.; Íñiguez, J.; Ghosez, P. Hybrid exchange-correlation functional for accurate prediction of the electronic and structural properties of ferroelectric oxides. *Phys. Rev. B: Condens. Matter Mater. Phys.* **2008**, *77*, 165107.
- (21) Schleck, R.; Nahas, Y.; Lobo, R. P. S. M.; Varignon, J.; Lepetit, M. B.; Nelson, C. S.; Moreira, R. L. Elastic and magnetic effects on the infrared phonon spectra of MnF₂. *Phys. Rev. B: Condens. Matter Mater. Phys.* **2010**, *82*, 054412.
- (22) Litvin, D. B. *Magnetic Group Tables*; International Union of Crystallography, 2013.
- (23) Kopsky, V.; Litvin, D. B. *International Tables for Crystallography Volume E: Subperiodic Groups*; Kluwer Academic Publishers: London, 2002.
- (24) Wang, D.; Liu, L.-M.; Zhao, S.-J.; Li, B.-H.; Liu, H.; Lang, X.-F. beta-MnO₂ as a cathode material for lithium ion batteries from first principles calculations. *Phys. Chem. Chem. Phys.* **2013**, *15*, 9075–9083.
- (25) Mackrodt, W. C.; Williamson, E.-A. First-principles description of the valence charge states in rutile MnO₂. *J. Chem. Soc., Faraday Trans.* **1997**, *93*, 3295–3300.
- (26) Franchini, C.; Podloucky, R.; Paier, J.; Marsman, M.; Kresse, G. Ground-state properties of multivalent manganese oxides: Density functional and hybrid density functional calculations. *Phys. Rev. B: Condens. Matter Mater. Phys.* **2007**, *75*, 195128.
- (27) Lim, J. S.; Saldana-Greco, D.; Rappe, A. M. Improved pseudopotential transferability for magnetic and electronic properties of binary manganese oxides from DFT+U+J calculations. *Phys. Rev. B* **2016**, *94*, 165151.
- (28) Lee, K.; Youn, Y.; Han, S. Identification of ground-state spin ordering in antiferromagnetic transition metal oxides using the Ising model and a genetic algorithm. *Sci. Technol. Adv. Mater.* **2017**, *18*, 246–252.
- (29) Dovesi, R.; Erba, A.; Orlando, R.; Zicovich-Wilson, C. M.; Civalleri, B.; Maschio, L.; Rerat, M.; Casassa, S.; Baima, J.; Salustro, S.; et al. Quantum-mechanical condensed matter simulations with CRYSTAL. *Wiley Interdiscip. Rev.: Comput. Mol. Sci.* **2018**, *8*, No. e1360.
- (30) Vilela Oliveira, D.; Laun, J.; Peintinger, M. F.; Bredow, T. BSSE-correction scheme for consistent gaussian basis sets of double- and triple-zeta valence with polarization quality for solid-state calculations. *J. Comput. Chem.* **2019**, *40*, 2364–2376.
- (31) Monkhorst, H. J.; Pack, J. D. Special points for Brillouin-zone integrations. *Phys. Rev. B: Solid State* **1976**, *13*, S188–S192.
- (32) Baur, W. H. Rutile-type compounds .5. Refinement of MnO₂ and MgF₂. *Acta Crystallogr., Sect. B: Struct. Sci.* **1976**, *32*, 2200–2204.
- (33) Regulski, M.; Przeniosło, R.; Sosnowska, I.; Hoffmann, J.-U. Incommensurate magnetic structure of beta-MnO₂. *Phys. Rev. B: Condens. Matter Mater. Phys.* **2003**, *68*, 172401.
- (34) Aroyo, M. I.; Perez-Mato, J. M.; Capillas, C.; Kroumova, E.; Ivantchev, S.; Madariaga, G.; Kirov, A.; Wondratschek, H. Bilbao Crystallographic Server: I. Databases and crystallographic computing programs. *Z. Kristallogr.* **2006**, *221*, 15–27.
- (35) Aroyo, M. I.; Kirov, A.; Capillas, C.; Perez-Mato, J. M.; Wondratschek, H. Bilbao Crystallographic Server. II. Representations of crystallographic point groups and space groups. *Acta Crystallogr., Sect. A: Found. Crystallogr.* **2006**, *62*, 115–128.
- (36) Aroyo, M. I.; Perez-Mato, J. M.; Orobengoa, D.; Tasci, E.; de la Flor, G.; Kirov, A. Crystallography online: Bilbao Crystallographic Server. *Bulg. Chem. Commun.* **2011**, *43*, 183–197.
- (37) Aroyo, M. I.; Orobengoa, D.; de la Flor, G.; Tasci, E. S.; Perez-Mato, J. M.; Wondratschek, H. Brillouin-zone database on the Bilbao Crystallographic Server. *Acta Crystallogr., Sect. A: Found. Adv.* **2014**, *70*, 126–137.
- (38) Yoshimori, A. A new type of antiferromagnetic structure in the rutile type crystal. *J. Phys. Soc. Jpn.* **1959**, *14*, 807–821.
- (39) Tompsett, D. A.; Parker, S. C.; Islam, M. S. Rutile (beta-)MnO₂ Surfaces and Vacancy Formation for High Electrochemical and Catalytic Performance. *J. Am. Chem. Soc.* **2014**, *136*, 1418–1426.
- (40) Tompsett, D. A.; Islam, M. S. Surfaces of Rutile MnO₂ Are Electronically Conducting, Whereas the Bulk Material Is Insulating. *J. Phys. Chem. C* **2014**, *118*, 25009–25015.
- (41) van Gog, H.; Li, W.-F.; Fang, C. M.; Koster, R. S.; Dijkstra, M.; van Huis, M. Thermal stability and electronic and magnetic properties of atomically thin 2D transition metal oxides. *npj 2D Mater. Appl.* **2019**, *3*, 18.
- (42) de la Flor, G.; Orobengoa, D.; Evarestov, R. A.; Kitaev, Y. E.; Tasci, E.; Aroyo, M. I. The site-symmetry induced representations of layer groups on the Bilbao Crystallographic Server. *J. Appl. Crystallogr.* **2019**, *52*, 1214–1221.
- (43) Janovec, V.; Litvin, D. B. Scanning of magnetic space groups and the analysis of non-magnetic domain walls. *Acta Crystallogr., Sect. A: Found. Crystallogr.* **2007**, *63*, 407–411.
- (44) Litvin, D. B.; Kopský, V. Space-group scanning tables. *Acta Crystallogr., Sect. A: Found. Crystallogr.* **2004**, *60*, 637.
- (45) Perez-Mato, J. M.; Gallego, S. V.; Tasci, E. S.; Elcoro, L.; de la Flor, G.; Aroyo, M. I. Symmetry-Based Computational Tools for Magnetic Crystallography. *Annu. Rev. Mater. Res.* **2015**, *45*, 217–248.